Efficiency Enhancement of Silicon Heterojunction Solar Cells via Photon Management Using Graphene Quantum Dot as Downconverters

Meng-Lin Tsai[†‡], **Wei-Chen Tu**[†], **Libin Tang**[§], **Tzu-Chiao Wei**[†], **Wan-Rou Wei**[†], **Shu Ping Lau**[§], **Lih-Juann Chen**[*‡], **and Jr-Hau He**[*†]

[†] Computer, Electrical and Mathematical Sciences and Engineering (CEMSE) Division, King Abdullah University of Science & Technology (KAUST), Thuwal 23955-6900, Kingdom of Saudi Arabia

[‡] Department of Materials Science and Engineering, National Tsing Hua University, Hsinchu 30013, Taiwan, Republic of China

[§] Department of Applied Physics, The Hong Kong Polytechnic University, Hung Hom, Hong Kong

Nano Lett., **2016**, *16* (1), pp 309–313

DOI: 10.1021/acs.nanolett.5b03814

Publication Date (Web): December 16, 2015

*E-mail: jrhau.he@kaust.edu.sa., *E-mail: ljchen@mx.nthu.edu.tw.

Abstract

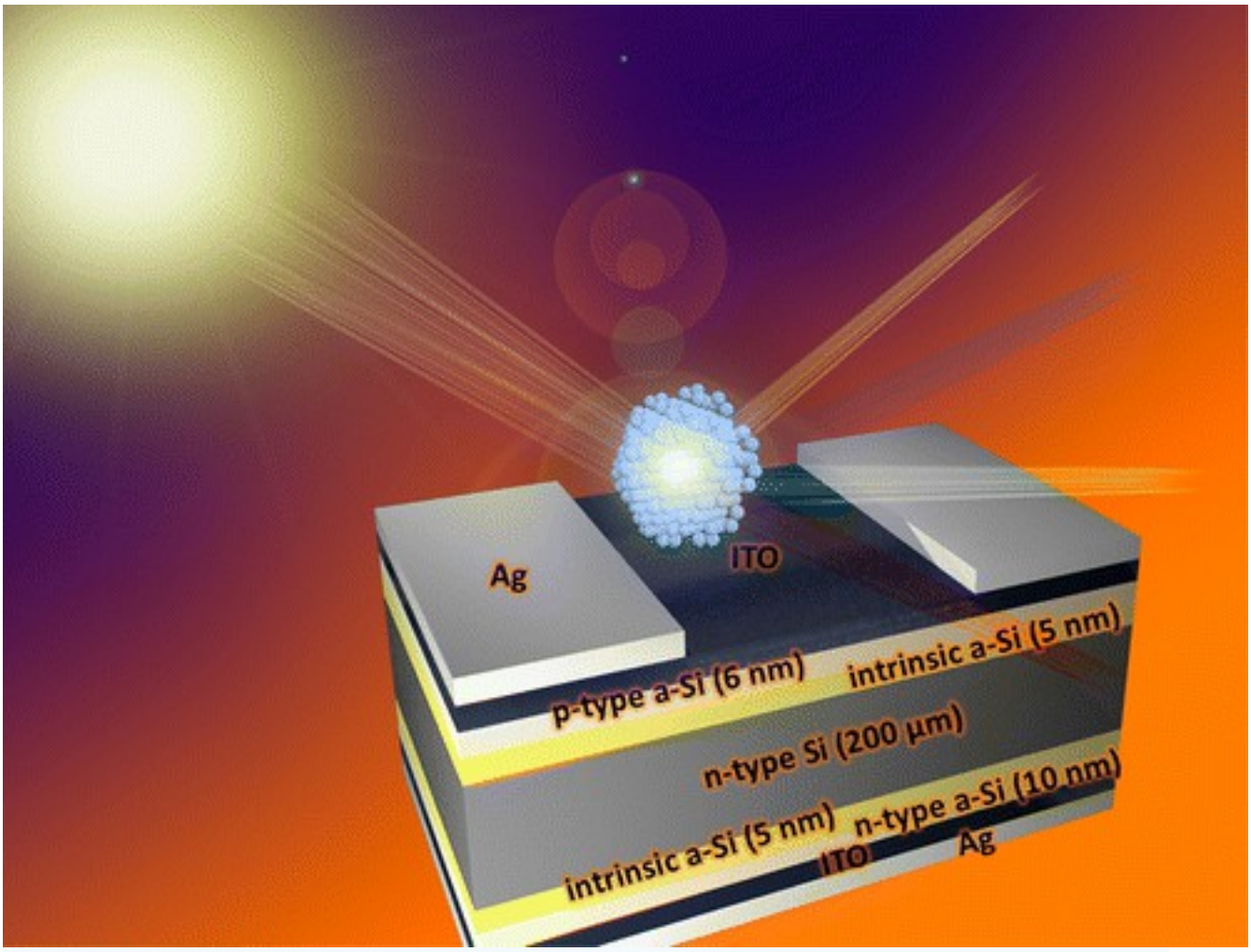

By employing graphene quantum dots (GQDs), we have achieved a high efficiency of 16.55% in n-type Si heterojunction solar cells. The efficiency enhancement is based on the photon downconversion phenomenon of GQDs to make more photons absorbed in the depletion region for effective carrier separation, leading to the enhanced photovoltaic effect. The short circuit current and the fill factor are increased from 35.31 to 37.47 mA/cm^2 and 70.29% to 72.51%, respectively. The work demonstrated here holds the promise for incorporating graphene-based materials in commercially available solar devices for developing ultrahigh efficiency photovoltaic cells in the future.

Keywords:
graphene; heterojunction; photovoltaic; quantum dot; solar cells

Graphene-based electronic and optoelectronic devices have been widely studied in the past decade due to the unique properties of graphene such as high mobility, low cost, transparency, and robustness. Impressive progress has been made, which includes using graphene as transparent

conductive electrodes in solar cells and see-through resistive random access memories.(1-3) The ultrahigh carrier mobility characteristic has also been utilized in developing transistors and ultrafast photodetectors.(4, 5) Moreover, it has been reported that in solar cell applications, graphene can serve as electrodes, carrier transport layers, and active layers of the device. For example, a graphene surface has been modified with polymer interlayers as the cathode of ZnO nanowire hybrid solar cells to achieve an efficiency of 4.2%.(1) Graphene nanoplatelets have also been applied as catalytic counter electrodes in dye-sensitized solar cells (DSSCs) with an efficiency of 9.3%.(2) Wang et al. have reported a remarkable method to develop low-temperature-processed graphene/TiO_2 electron collection layers of thin film perovskite solar cells, which exhibits an efficiency of 15.6%.(6) In addition, graphene has also been used to form Schottky junctions with TiO_2 and n-type Si in DSSC and Schottky junction solar cells with efficiencies up to 6.06% and 8.6%, respectively.(7, 8) Recently, MoS_2/graphene monolayer-based solar cells have been fabricated to exhibit ultrahigh power density per kilogram.(9) Photovoltaic devices based on WSe_2–MoS_2 2D lateral p–n heterojunction have also been demonstrated to exhibit a power conversion efficiency (PCE) of 0.2%.(10) However, the absorption in these fully monolayer-based materials is limited, leading to the unsatisfactory efficiency or restricted absorption range. To further realize graphene in high efficiency industrial applications, the integration of graphene-based materials with commercially available ultrahigh efficiency solar materials has become an important task and warrants further investigation.

Graphene quantum dots (GQDs), exhibiting unique semiconducting properties, have becoming a newly emerged material for optoelectronic applications.(11, 12) The bandgap of GQDs can be tuned by adjusting their chemical functional groups.(12) Additionally, the most intriguing feature of GQDs for optical applications is the photon downconversion property, which enables them to absorb photons in shorter wavelength regions and then emit photons in longer wavelength regions.(11, 12) Employing photon downconverters with multiple electron–hole pairs generated per incident photon could possibly exceed the Shockley–Queisser limit, the maximum theoretical efficiency of a solar cell.(13) The downconversion phenomenon has been observed in rare earth materials and some II–VI semiconductor nanoparticles, which are usually costly.(14) However, GQDs are excellent alternative of downconverter materials because of abundant carbon on earth. In addition to their distinguished optical properties, GQDs can further enhance the conductivity of the organic layers due to the inherent high mobility of graphene to improve electrical properties of the device. The superior solubility of GQDs in aqueous solution can also be integrated well with other commercially

available fabrication processes and becomes more suitable than typical layered 2D materials to be uniformly deposited on a variety of surface structures such as micropyramids or nanowires.

Si-based solar cells have dominated the commercial photovoltaic (PV) market in the past decades due to high abundance of Si materials, high efficiency, and mature Si semiconductor technologies. For achieving ultrahigh efficiencies in Si-based devices, Si heterojunction (SHJ) solar cells using n-type substrates have attracted much attention in recent years. In April of 2014, Panasonic has announced a high efficiency of 25.6% in its heterojunction with intrinsic thin-layer (known as HIT) cells among all kinds of Si-based solar cells of practical size (100 cm^2 and above).(15) Compared with p-type Si solar cells, n-type Si solar cells possess enormous advantages in terms of efficiency and cost effectiveness including suitable band structure, high minority carrier lifetimes (up to the millisecond range), no light-induced degradation caused by boron–oxygen pair, and high impurity tolerance.(16-21) Despite the great success in developing high performance SHJ devices, a large number of photons are still wasted, leading to the significant power loss. It is reported that the total power loss is more than 20% of the current output power. As a consequence, there is a growing interest in the scientific research and the industrial implementation of n-type SHJ-based PV technologies with photon management strategies. Previously, by designing SHJ solar cells with photon management schemes using various hierarchical structures, the high efficiencies of 15.14% (nanowires on micropyramids) and 15.2% (micropyramids on microgrooves) with excellent omnidirectionality have been achieved.(20, 21) Related works on n-type SHJ-based PV technologies with photon management methods for the past years are summarized in Table S1 in Supporting Information. Another major factor for the power loss is the light absorption loss in the a-Si.(22) Only 30% of light absorbed in the a-Si:H layer contributes to the short-circuit current due to the high defect density in a-Si:H layers. It is known that most of the UV radiation produces electron–hole pairs near the surface, severe recombination would occur in the a-Si:H layer due to the high defect density. In order to reduce the defect density in a-Si:H layers or the thickness of the device, additional chemical polishing, etching, or fabrication of ultrathin oxide layers has been applied.(20) However, these would increase cost and complexity of the fabrication process. Therefore, an alternative way to reduce the power loss is using downconversion materials such as GQDs to convert light in the UV region to light in the visible region. The extinction distance of the visible light is longer than that of the UV light, which increases the probability that the photons reach the monocrystalline Si layer to reduce power loss.

In the present study, the introduction of GQDs to n-type SHJ solar cells leads to the increase of short-circuit current (J_{sc}) from 35.31 mA/cm^2 to 37.47 mA/cm^2 and fill factor (FF) from 70.29% to 72.51% due to the photon downconversion effect of GQDs to absorb UV light (which originally would be absorbed in the high-defect-density a-Si:H layer and be wasted) and convert UV photons into visible photons. The optical improvement due to the downconversion effect of GQDs gives rise to a high efficiency of 16.55%. The realization of high-efficiency GQD-based SHJ solar cells demonstrated here makes GQDs attractive for large area, high efficiency, and commercially available cell production.

Micropyramidal Si surfaces were fabricated on as-cut Czochralski (CZ) n-type monocrystalline Si (001) wafers by anisotropic chemical etching in a solution of potassium hydroxide (KOH, 45 vol %) and isopropyl alcohol (IPA) at 85 °C for 20 min. The PECVD process was carried out at 150 °C for the deposition of intrinsic a-Si:H buffer layer (5 nm)/p-type a-Si:H layer (6 nm) on top as emitter layers, and intrinsic a-Si:H buffer layer (5 nm)/n-type a-Si:H layer (10 nm) on the back as surface field layers. ITO contacts were deposited on both sides by the sputtering method, followed by Ag grids on the top and a full coverage of Ag on the back using the electron beam evaporation. Finally, various concentrations of GQDs were spin-coated on top of SHJ devices at 800 rpm for 90 s. A commercial scanning electron microscope (JEOL JSM-6500 Field Emission SEM) has been utilized to investigate the morphology of the substrate. Absorbance and haze spectra were measured for wavelength region between 200 and 1200 nm under a UV–vis-NIR spectrometer (JASCO ARN-733) with an integrating sphere and a noise level of 0.002%. Current density–voltage (*J*–*V*) characteristics were measured using an Agilent B2902A precision source/measure unit. External quantum efficiency (EQE) measurement has been carried out with a spectral response system (Enli Technology Co., Ltd. R3011) for the wavelengths ranging from 300 to 1000 nm.

Water-soluble GQDs were prepared by using glucose and DI water as solute and solvent, respectively.(11) The solution was heated with a microwave oven at 700 W for 11 min and cooled down to room temperature for further device fabrication and characterizations. On the basis of the previous work, the fluorescence quantum yields of GQDs are in the range of 7–11%.(11) The height of the GQDs was characterized by atomic force microscope (AFM) (Digital Instrumennts NanoScope IV) operated in the tapping mode. Transmission electron microscopy (TEM) and high resolution TEM (HRTEM) were performed on JEOL JEM-2100F at an operating voltage of 200 kV. Raman scattering spectrum was obtained using a Horiba Jobin Yvon HR800 spectrometer with an excitation laser at a

wavelength of 488 nm. Photoluminescence (PL) and PL excitation (PLE) measurements were carried out using a Hitachi F-4500 fluorescence spectrophotometer.

Figure 1a shows the AFM image of GQDs. The size of the GQDs can be quantitatively characterized. As shown in the inset of Figure 1a, the diameter of the GQD in red circle A is around 3.4 nm. To reveal the structure of GQDs more clearly, Figure 1b shows the TEM image of GQDs assembled on carbon film-covered Cu grids. It is shown that the diameter of the GQDs is consistent with the results from the AFM profile. From the HRTEM images in the inset of Figure 1b, GQDs exhibit 0.364 nm fringes corresponding to the *d* spacing between graphene layers, which are slightly larger than the basal plane distance of bulk graphite (0.335 nm).(23) This can be attributed to the presence of functional groups at the edges of the GQDs. Raman spectroscopy has also been used to characterize GQDs, as shown in Figure 1c. Two significant peaks around 1340 and 1580 cm^{-1} represent D band and G band, respectively, which can be used to confirm the formation of GQDs.(24) In addition, photoluminescence emission (PLE), photoluminescence (PL), and absorbance spectra measurements have been carried out to characterize the optical behavior of GQDs.
In Figure 1d, the PL spectrum of GQDs is measured under the excitation wavelength of 375 nm. The PLE spectrum measured at the emission peak of PL (453 nm) shows an excitation peak at 367 nm. The above results indicate the downconversion behavior of GQDs, which is the ability to absorb light from the UV region and emit light in the visible region. Figure 1e shows the absorbance spectrum of GQDs on the glass substrate. It is shown that GQDs mainly absorb light in the UV region, which is consistent with the PLE spectrum. In the visible region, GQDs remain transparent. Therefore, photons in the visible region can reach the depletion region of the Si substrate successfully without being absorbed by GQDs.

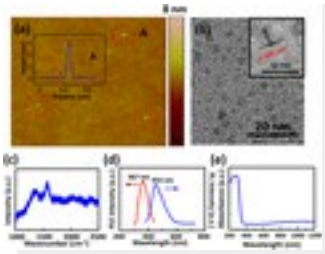

Figure 1. (a) AFM image, (b) TEM and HRTEM (inset) images, (c) Raman spectrum, (d) PLE (left) and PL (right) spectra, and (e) absorbance spectrum of GQDs.

To gain insight into the downconversion behavior of GQDs, we have measured the haze (H_T) spectrum of 0.3 wt % GQDs on the glass substrate, as shown in Figure 2. The haze can be

$$H_T = \frac{T_{diff}}{T_{total}} \times 100\%$$

expressed as where T_{diff}, T_{total}, and $T_{specular}$ denote diffused, total, and specular transmittance, respectively and $T_{diff} = T_{total} - T_{specular}$. It is shown that H_T is below 1% from 400 to 1200 nm, showing negligible light scattering throughout the visible and infrared regions. The peak at 350 nm can be attributed to the downconversion behavior of GQDs. Light in this region is first absorbed by the GQDs and then emitted in various directions toward the surrounding. Accordingly, the downconversion property in the UV region makes GQDs applicable for enhancing solar cell device performances.

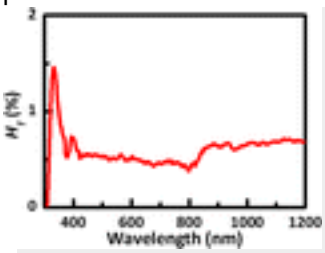

Figure 2. Haze spectrum of 0.3 wt % GQDs on glass substrates.

The photographic image and the cross-sectional schematic of the SHJ solar cell are shown in Figure 3a and b, respectively. The SHJ solar cell is fabricated by using as-cut CZ n-type substrates to save the production cost and show its feasibility for mass production. Si micropyramids were fabricated via an anisotropic etching process using a solution of KOH and IPA. Figure 3c and d shows the low-magnification and high-magnification top-view SEM images of the micropyramids, respectively. Figure 3e shows the cross-sectional SEM image of the micropyramids. Due to the high water solubility of GQDs, they can be well spin-coated on top of various surface structures. After the formation of SHJ solar cells, GQDs were spin-coated on top of the device and dried in ambient air for further characterization. The actual cell size for measurement is 4 cm^2.

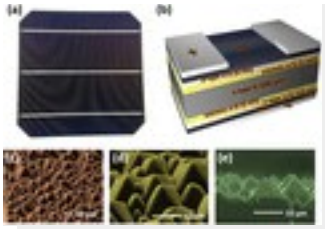

Figure 3. (a) Photographic image, (b) schematic, (c) low-resolution, (d) high-resolution, and (e) cross-sectional SEM images of SHJ solar cells.

After sequential device fabrication processes, *J–V* characteristics of SHJ devices with various concentrations of GQDs were measured under the AM 1.5G illumination, as shown in Figure 4a. The

measured photovoltaic parameters are summarized in Table 1. It is shown that for the concentration below 0.3 wt %, higher concentration of GQDs leads to higher J_{sc}, indicating that more UV photons are absorbed and downconverted by GQDs and downconverted photons are collected by the depletion region of SHJ. The device with 0.3 wt % of GQDs shows the highest J_{sc} and FF of 37.47 mA/cm^2 and 72.51%, respectively, leading to the highest PCE of 16.55%. However, for the concentration of GQDs over 0.3 wt %, performance degradation of the SHJ devices was observed. It has been reported that a thicker GQD layer can lead to poor electrical conductivity, which results in degraded J_{sc}, FF, and PCE.(25) The EQE of the devices with 0.3 wt % and without GQDs and the EQE enhancement are shown in Figure 4b and c, respectively. The EQE enhancement is defined as the EQE of the device with 0.3 wt % GQDs divided by that of the device without GQDs. In Figure 4c, the significant EQE enhancement peak of up to 11% at 370 nm, whereas broadband EQE enhancement (up to 4%) is observed from 400 to 1000 nm. This can be attributed to the downconversion behavior of GQDs at the UV region and the broadband antireflection properties of GQDs. Because most of the incident UV photons produce photogenerated carriers near the surface, the photogenerated carriers could easily recombine in the presence of defects in the a-Si:H layer and between layer interfaces, leading to poor quantum efficiencies at UV regions. With the addition of GQDs facilitating the downconversion effect on SHJ cells, more photons with long wavelengths can be absorbed and excite carriers in the depletion region for immediate photogenerated carrier separation due to the built-in electric field, leading to the increased photovoltaic effect. In addition, it has been reported that QDs can increase the surface roughness of the device surface, leading to broadband EQE enhancement of solar cells.(14, 26)

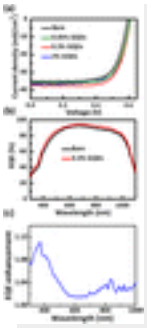

Figure 4. (a) *J*–*V* characteristics of SHJ solar cells with various concentration of GQDs. (b) EQE spectra of SHJ solar cells without and with 0.3 wt % of GQDs. (c) EQE enhancement spectrum of SHJ solar cell with 0.3 wt % of GQDs.

Table 1. Photovoltaic Parameters of SHJ Solar Cells with Various Concentrations of GQDs

GQD concentration	V_{OC} (V)	J_{SC} (mA/cm^2)	FF (%)	PCE (%)
bare	0.60	35.31	70.29	14.77
0.05%	0.61	36.05	71.19	15.66
0.1%	0.61	37.25	72.23	16.50
0.3%	0.61	37.47	72.51	16.55
0.7%	0.61	37.43	72.07	16.45
1%	0.61	37.27	71.71	16.30
2%	0.61	36.30	70.49	15.60

We have successfully fabricated n-type SHJ solar cells with the efficiency up to 16.55% by employing the downconversion effect of GQDs. Because the expansion of operating spectral range toward the UV region, the GQD downconverters can help in harvesting the full solar energy and thus increase the photovoltaic effect, giving rise to the increase in J_{SC} and FF of the SHJ solar cells with 0.3 wt % GQDs from 35.31 to 37.47 mA/cm^2 and from 70.29% to 72.51%, respectively. This photon management scheme via downconversion effect of GQDs successfully implemented into wafer-scale

Si cell fabrication processes would hold the promise for achieving large-area and cost-effective solar cell production.

Supporting Information

The Supporting Information is available free of charge on the ACS Publications website at DOI: 10.1021/acs.nanolett.5b03814.

- The photovoltaic characteristics of n-type Si heterojunction solar cells with photon management methods. (PDF)

- **PDF**
  - nl5b03814_si_001.pdf (145.04 kB)

Efficiency Enhancement of Silicon Heterojunction Solar Cells via Photon Management Using Graphene Quantum Dot as Downconverters

figshare

ShareDownload

Author Contributions

The first two authors, Meng-Lin Tsai and Wei-Chen, contributed equally to this work.

The authors declare no competing financial interest.

Acknowledgment

The work was supported by the Research Grants Council of Hong Kong (Project no. PolyU 153012/14P) and National Natural Science Foundation of China (NSFC grant no. 11374250).

- Reference QuickView

References

This article references 26 other publications.

1. 1.

   Park, H.; Chang, S.; Jean, J.; Cheng, J. J.; Araujo, P. T.; Wang, M. S.; Bawendi, M. G.; Dresselhaus, M. L.;Bulovic, V.; Kong, J.; Gradecak, S. *Nano Lett.* **2013**, 13, 233– 239 DOI: 10.1021/nl303920b

   [ACS Full Text], [CAS]

2. 2.

   Kavan, L.; Yum, J. H.; Nazeeruddin, M. K.; Grätzel, M. *ACS Nano* **2011**, 5, 9171– 9178 DOI: 10.1021/nn203416d

   [ACS Full Text], [CAS]

3. 3.

   Yang, P. K.; Chang, W. Y.; Teng, P. Y.; Jeng, S. F.; Lin, S. J.; Chiu, P. W.; He, J. H. *Proc. IEEE* **2013**, 101,1732– 1739 DOI: 10.1109/JPROC.2013.2260112

   [Crossref], [CAS]

4. 4.

   Schwierz, F. *Nat. Nanotechnol.* **2010**, 5, 487– 496 DOI: 10.1038/nnano.2010.89

   [Crossref], [PubMed], [CAS]

5. 5.

   Xia, F.; Mueller, T.; Lin, Y. M.; Valdes-Garcia, A.; Avouris, P. *Nat. Nanotechnol.* **2009**, 4, 839– 843 DOI: 10.1038/nnano.2009.292

   [Crossref], [PubMed], [CAS]

6. 6.

   Wang, J. T. W.; Ball, J. M.; Barea, E. M.; Abate, A.; Alexander-Webber, J. A.; Huang, J.; Saliba, M.;Mora-Sero, I.; Bisquert, J.; Snaith, H. J.; Nicholas, R. J. *Nano Lett.* **2014**, 14, 724– 730 DOI: 10.1021/nl403997a

   [ACS Full Text], [CAS]

7. 7.

   Song, J.; Yin, Z.; Yang, Z.; Amaladass, P.; Wu, S.; Ye, J.; Zhao, Y.; Deng, W. Q.; Zhang, H.; Liu, X. W.*Chem. - Eur. J.* **2011**, 17, 10832– 10837 DOI: 10.1002/chem.201101263

   [Crossref], [PubMed], [CAS]

8. 8.

Miao, X.; Tongay, S.; Petterson, M. K.; Berke, K.; Rinzler, A. G.; Appleton, B. R.; Hebard, A. F. *Nano Lett.***2012**, 12, 2745– 2750 DOI: 10.1021/nl204414u

[ACS Full Text], [CAS]

9. 9.

Bernardi, M.; Palummo, M.; Grossman, J. C. *Nano Lett.* **2013**, 13, 3664– 3670 DOI: 10.1021/nl401544y

[ACS Full Text], [CAS]

10. 10.

Li, M. Y.; Shi, Y.; Cheng, C. C.; Lu, L. S.; Lin, Y. C.; Tang, H. L.; Tsai, M. L.; Chu, C. W.; Wei, K. H.; He, J. H.;Chang, W. H.; Suenaga, K.; Li, L. J. *Science* **2015**, 349, 524– 528 DOI: 10.1126/science.aab4097

[Crossref], [PubMed], [CAS]

11. 11.

Tang, L.; Ji, R.; Cao, X.; Lin, J.; Jiang, H.; Li, X.; Teng, K. S.; Luk, C. M.; Zeng, S.; Hao, J.; Lau, S. P. *ACS Nano* **2012**, 6, 5102– 5110 DOI: 10.1021/nn300760g

[ACS Full Text], [CAS]

12. 12.

Kim, J. K.; Park, M. J.; Kim, S. J.; Wang, D. H.; Cho, S. P.; Bae, S.; Park, J. H.; Hong, B. H. *ACS Nano***2013**, 7, 7207– 7212 DOI: 10.1021/nn402606v

[ACS Full Text], [CAS]

13. 13.

Shockley, W.; Queisser, H. J. *J. Appl. Phys.* **1961**, 32, 510– 519 DOI: 10.1063/1.1736034

[Crossref], [CAS]

14. 14.

Huang, C. Y.; Wang, D. Y.; Wang, C. H.; Chen, Y. T.; Wang, Y. T.; Jiang, Y. T.; Yang, Y. J.; Chen, C. C.;Chen, Y. F. *ACS Nano* **2010**, 4, 5849– 5854 DOI: 10.1021/nn101817s

[ACS Full Text], [CAS]

15. 15.

Panasonic HIT Solar Cell Achieves World's Highest Energy Conversion Efficiency of 25.6% at Research Level. http://panasonic.co.jp/corp/news/official.data/data.dir/2014/04/en140410-4/en140410-4.html(accessed Nov 30, **2015**) .

16. 16.

Descoeudres, A.; Holman, Z. C.; Barraud, L.; Morel, S.; De Wolf, S.; Ballif, C. *IEEE J. Photovoltaics* **2013**, 3,83– 89 DOI: 10.1109/JPHOTOV.2012.2209407

[Crossref]

17. 17.

Cuevas, A.; Kerr, M. J.; Samundsett, C.; Ferrazza, F.; Coletti, G. *Appl. Phys. Lett.* **2002**, 81, 4952– 4954DOI: 10.1063/1.1529089

[Crossref], [CAS]

18. 18.

Glunz, S. W.; Rein, S.; Lee, J. Y.; Warta, W. *J. Appl. Phys.* **2001**, 90, 2397– 2404 DOI: 10.1063/1.1389076

[Crossref], [CAS]

19. 19.

Geerligs, L. J.; Macdonald, D. *Prog. Photovoltaics* **2004**, 12, 309– 316 DOI: 10.1002/pip.546

[Crossref], [CAS]

20. 20.

Wang, H. P.; Lin, T. Y.; Hsu, C. W.; Tsai, M. L.; Huang, C. H.; Wei, W. R.; Huang, M. Y.; Chien, Y. J.;Yang, P. C.; Liu, C. W.; Chou, L. J.; He, J. H. *ACS Nano* **2013**, 7, 9325– 9335 DOI: 10.1021/nn404015y

[ACS Full Text], [CAS]

21. 21.

Wang, H. P.; Lin, T. Y.; Tsai, M. L.; Tu, W. C.; Huang, M. Y.; Liu, C. W.; Chueh, Y. L.; He, J. H. *ACS Nano***2014**, 8, 2959– 2969 DOI: 10.1021/nn500257g

[ACS Full Text], [CAS]

22. 22.

Mishima, T.; Taguchi, M.; Sakata, H.; Maruyama, E. *Sol. Energy Mater. Sol. Cells* **2011**, 95, 18– 21 DOI: 10.1016/j.solmat.2010.04.030

[Crossref]

23. 23.

Oshima, C.; Nagashima, A. *J. Phys.: Condens. Matter* **1997**, 9, 1– 20 DOI: 10.1088/0953-8984/9/1/004

[Crossref], [CAS]

24. 24.

Tuinstra, F.; Koenig, J. L. *J. Chem. Phys.* **1970**, 53, 1126 DOI: 10.1063/1.1674108

[Crossref], [CAS]

25. 25.

Gao, P.; Ding, K.; Wang, Y.; Ruan, K.; Diao, S.; Zhang, Q.; Sun, B.; Jie, J. *J. Phys. Chem. C* **2014**, 118,5164– 5171 DOI: 10.1021/jp412591k

[ACS Full Text], [CAS]

26. 26.

Jacobsson, T. J.; Edvinsson, T. *RSC Adv.* **2012**, 2, 10298– 10305 DOI: 10.1039/c2ra21566g

[Crossref], [CAS]